

# One-Shot Object Localization in Medical Images based on Relative Position Regression

Wenhui Lei<sup>1</sup>, Wei Xu<sup>1</sup>, Ran Gu<sup>1</sup>, Hao Fu<sup>1</sup>, Shaoting Zhang<sup>1,2</sup>, and  
Guotai Wang<sup>1\*</sup>

<sup>1</sup>School of Mechanical and Electrical Engineering, University of Electronic Science  
and Technology of China, Chengdu, China

<sup>2</sup>SenseTime Research, Shanghai, China  
guotai.wang@uestc.edu.cn

**Abstract.** Deep learning networks have shown promising performance for accurate object localization in medical images, but require large amount of annotated data for supervised training, which is expensive and expertise burdensome. To address this problem, we present a one-shot framework for organ and landmark localization in volumetric medical images, which does not need any annotation during the *training* stage and could be employed to locate any landmarks or organs in test images given a support (reference) image during the *inference* stage. Our main idea comes from that tissues and organs from different human bodies have a similar relative position and context. Therefore, we could predict the relative positions of their non-local patches, thus locate the target organ. Our framework is composed of three parts: (1) A projection network trained to predict the 3D offset between any two patches from the same volume, where human annotations are not required. In the inference stage, it takes one given landmark in a reference image as a support patch and predicts the offset from a random patch to the corresponding landmark in the test (query) volume. (2) A coarse-to-fine framework contains two projection networks, providing more accurate localization of the target. (3) Based on the coarse-to-fine model, we transfer the organ bounding-box (B-box) detection to locating six extreme points along x, y and z directions in the query volume. Experiments on multi-organ localization from head-and-neck (HaN) CT volumes showed that our method acquired competitive performance in real time, which is more accurate and  $10^5$  times faster than template matching methods with the same setting. Code is available: <https://github.com/LWHYC/RPR-Loc>.

**Keywords:** Medical Images · One-shot Localization · Relative Position

## 1 Introduction

Accurate localization of organs and anatomical landmarks is crucial in medical image analysis, as it can assist in the treatment, diagnosis and follow-up of

\* Correspond author.

First Author and Second Author contribute equally to this work.

many diseases [17]. Nowadays, Deep Learning (DL) has achieved state-of-the-art performance in the localization of a broad of structures, including abdominal organs [16], brain tissues [14], thoracic organs [6], etc. However, their success mainly relies on a large set of annotated images for training, which is expensive and time-consuming to acquire, and can hardly be obtained when access to experts are limited.

To address this problem, reducing the demand on human annotations for training has recently attracted increasing attentions. Among several techniques such as weakly supervised [12] and semi-supervised learning [15], one-shot learning (OSL) is appealing as it does not require annotations of the target during training, and only needs one annotated support image at the inference time [2, 4]. Typical OSL methods follow a support-query framework, in which an existing model generalizes to an unknown class with only one example (usually denoted as support) to make predictions for testing examples (usually denoted as query). It could have a large impact on annotation-efficient medical image analysis because it addresses learning from scarcely annotated data. However, to the best of our knowledge, there have been very few works on one-shot object localization in volumetric medical scans, such as Computed Tomography (CT) and Magnetic Resonance Images (MRI). In addition, despite that existing OSL methods do not require annotations of the target object during training, they follow a meta-learning strategy [11] and require a large set of annotated images of several other objects, which is still limited by access to these annotations.

Different from existing works, we get rid of meta-learning and propose a novel one-shot localization method based on Relative Position Regression (RPR-Loc) for organ/landmark localization in volumetric medical images. It does not require annotations of either the target organs or other types of objects during training. In the inference stage, it can be directly used to locate any landmarks or organs that are specified by a support (reference) image. In contrast, template matching [3] could also be used for object localization given a reference image, i.e., the template. However, the matching process is time-consuming due to the sliding window scanning and therefore not suitable for real-time applications.

Our main inspiration comes from the fact that the spatial distributions of organs (landmarks) have strong similarities among patients. First, different structures among persons have very similar relative positions [5], such as in the case of head and neck CT images, which makes it possible to predict the relative position (i.e., offset) between two patches in a volume. Second, the same landmark across different persons has very similar local context, which allows us to use a given landmark in a support image as reference to find the corresponding one in a test image. With a set of training images without annotations, we train a network to predict the 3D offset in the physical space between any two patches of the same volume. At the inference stage, we use the network to predict the offset from an agent’s current position (represented by the patch centered on it) to the target landmark position in the test image, which is approximately represented by a patch centered on the corresponding position in an annotated support image,

based on the assumption that the patches centered on corresponding landmarks between different patients are similar.

The contribution of this work is summarized as follows. First, our proposed one-shot localization framework RPR-Loc casts an organ localization task to locating a set of landmarks, i.e., the extreme points, and the landmark localization is modeled as an offset regression problem. Second, we propose a projection network (Pnet) that is trained to predict the 3D offset between any two patches from the same image. We represent the bounding box of a target object by six extreme points, and locate these extreme points respectively by using Pnet to predict the offset from an agent’s current position to the target position. Thirdly, we propose a coarse-to-fine framework based on Pnet that allows an agent to move multiple steps for accurate localization, and introduce a multi-run ensemble strategy to further improve the performance. Therefore, our method removes the need of human annotations of the training images.

## 2 Methodology

Our proposed RPR-Loc for one-shot object localization is illustrated in Fig. 1. Given a certain reference landmark in a support image, an agent tries to find the corresponding target landmark in the test (query) image. A network called Pnet takes a patch around the reference landmark (i.e., support patch) and a patch centered at the agent’s current position (moving patch, a.k.a., query patch) as input, and infers the offset from the moving patch to the target patch centered on the target landmark in the test image corresponding to the reference landmark. The bounding box (B-Box) of an organ is obtained by locating its six extreme points along x, y and z axes with the help of the annotated support/reference image. Note that when locating each extreme point, the agent can move multiple steps following a coarse-to-fine workflow to obtain more accurate results.

The structure of this section is arranged as follows. In Section 2.1, we describe our Pnet for offset regression between two patches and how it is used for landmark localization. In Section 2.2, we introduce multi-step localization and multi-run ensemble for accurate and robust localization. In Section 2.3, the implementation of organ detection based on localization of extreme points is detailed.

### 2.1 Relative Position Regression and Projection Network

Let  $\mathbf{v}$  denote a volumetric image in the unannotated training set, and let  $\mathbf{x}_q$  and  $\mathbf{x}_s$  represent a moving (query) patch and a reference (support) patch in  $\mathbf{v}$  respectively, we use a network to predict the 3D offset from  $\mathbf{x}_q$  to  $\mathbf{x}_s$ . Assuming the pixel spacing of  $\mathbf{v}$  is  $\mathbf{e} \in R^3$  while  $\mathbf{c}_q, \mathbf{c}_s \in R^3$  represent the centroid coordinates of  $\mathbf{x}_q$  and  $\mathbf{x}_s$  in the image space, the ground truth offset  $\mathbf{d}'_{qs}$  from  $\mathbf{x}_q$  to  $\mathbf{x}_s$  in the physical space is denoted as:

$$\mathbf{d}'_{qs} = (\mathbf{c}_s - \mathbf{c}_q) \circ \mathbf{e} \quad (1)$$

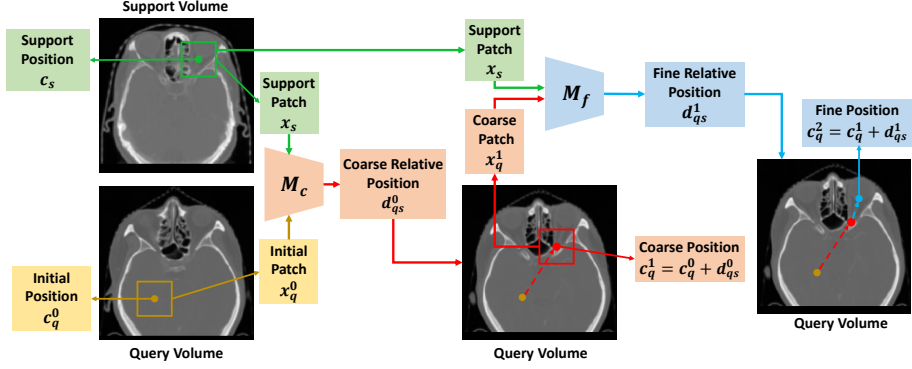


Fig. 1: Proposed one-shot localization method based on Relative Position Regression (RPR-Loc). The green box represents a support (reference) patch in the support image that specifies a landmark to locate in a test image, and the yellow box is an initial patch that represents the current position of an agent in the test image.  $M_c$  (coarse projection net) takes the support patch and initial patch as input to regress the offset from the initial patch to the desired landmark in the test image. The agent moves one step given by the offset, and its new position is represented by the red box, which is a coarse result of the localization. We apply the  $M_f$  (fine projection net) to obtain a fine localization result given the agent’s new position and the support patch.

where  $\circ$  represents the element-wise product.

As shown in Fig. 2, the size of  $x_s$  and  $x_q$  is  $16 \times 64 \times 64$  pixels when dealing with Head and Neck CT images with high inter-slice spacing. Our Pnet takes  $x_s$  and  $x_q$  as input and predicts their 3D offset. We use a shared projection encoder to transform  $x_s$  and  $x_q$  to a latent vector  $p_s$  and  $p_q$ , respectively. The shared encoder is composed of two parts: five convolution blocks to extract high-level features and three fully connected layers mapping the high-level features to a 3D latent vector. Considering the large inter-slice spacing, we use one inter-slice convolution after three intra-slice convolutions in each convolution block. The feature extractor uses three max-pooling layers to reduce the spatial resolution and capture global features in the patch.

With the hidden vectors  $p_s$  and  $p_q$ , the predicted offset  $d_{qs} \in R^3$  from the query patch  $x_q$  to the support patch  $x_s$  is obtained as:

$$d_{qs} = r \times \tanh(p_s - p_q) \quad (2)$$

where the hyperbolic tangent function  $\tanh$  and the hyper-parameter  $r$  together control the upper and lower bound of  $d_{qs}$ , which is set to cover the largest possible offset. Finally, we apply the mean square error (MSE) loss function to measure the difference between  $d_{qs}$  and  $d'_{qs}$ :

$$Loss = ||d_{qs} - d'_{qs}||^2 \quad (3)$$

In the inference stage for landmark localization, we use an annotated support (reference) image to specify the desired landmark, and aim to find the position of

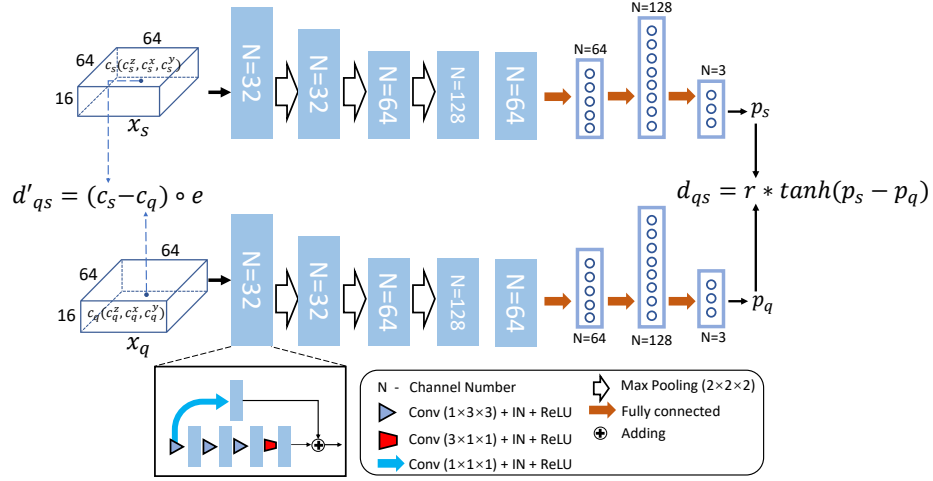


Fig. 2: Structure of our projection network (Pnet) for offset prediction.  $x_s$  and  $x_q$  are the support and query patches centered at positions  $c_s$  and  $c_q$  respectively. We use a shared encoder to transform  $x_s$  and  $x_q$  to 3D latent vectors  $p_s$  and  $p_q$ , respectively. The shared encoder contains five convolution layers and three fully connected layers. We apply scale factor  $r$  and hyperbolic tangent function  $\tanh$  to get the predicted offset  $d_{qs}$ , i.e., relative position from  $x_s$  to  $x_q$ .

the corresponding landmark in a test image. The problem is modeled as moving an agent from a random initial position to the target position. Therefore, we take a patch at a random position  $c_0 \in R^3$  in the test image as  $x_q$ , which is the initial status of the agent, and take the patch centered at the specified landmark in the support image as the support patch, which is an approximation of the unknown target patch in the test image and serves as  $x_s$ . By applying Pnet with  $x_s$  and  $x_q$ , we obtain an offset  $d_{qs} \in R^3$ , thus we move the agent with  $d_{qs}$ , and obtain  $c = c_0 + d_{qs}$  as the detected landmark position in the test image. It should be noted that, for more accurate detection, the movement of the agent is not limited to one step, which is detailed in the following.

## 2.2 Multi-Step Localization and Multi-Run Ensemble

**Multi-step localization** As moving the localization agent with only one step from the initialized position towards the target position may not be accurate enough, our framework supports moving the agent by multiple steps, i.e., Pnet can be applied several times given the agent's new position and the support patch. We find that moving three steps does not obviously perform better than two steps, therefore we employ two-step inference strategy. The first step obtains a coarse localization, where the offset can be very large. The second step obtains a fine localization with a small offset around the coarse localization result.

To further improve the performance, we train two models for these two steps respectively. More specifically, during training of the coarse location model  $M_c$ , we crop  $x_q$  and  $x_s$  randomly across the entire image space. And we set  $r = 300$

to cover the largest possible offset. For the fine model  $M_f$ , we crop the  $x_q$  and  $x_s$  in a random local area, and limit their maximal distance to be  $r = 30$ . Therefore,  $M_c$  could handle large movements at the beginning while  $M_f$  then focuses on the movement with small steps.

During the inference stage, we utilize  $M_c$  and  $M_f$  to move the agent in the first and second steps, respectively. Given a support patch  $x_s$  in a reference image and the agent's initial position  $c_q^0$  (with the corresponding patch  $x_q^0$ ) in the test image, we use  $M_c$  taking  $x_q^0, x_s$  as input to obtain a coarse offset  $d_{qs}^0$  in the test image, and the agent's position is updated as  $c_q^1 = c_q^0 + d_{qs}^0$ . Let  $x_q^1$  denote the patch at  $c_q^1$ . Based on  $x_q^1$  and  $x_s$ ,  $M_f$  predicts a fine offset  $d_{qs}^1$ . Thus, the predicted location of the target landmark is  $c_q^2 = c_q^1 + d_{qs}^1$ .

**Multi-run ensemble** As the position of the agent during inference is initialized randomly, different initialization may obtain slightly different results. To obtain more robust results, we propose a multi-run ensemble strategy: we locate each target landmark  $K$  times with different random initializations, and average the localization results.

### 2.3 Organ Detection via Landmark Localization

Section 2.2 has described how to use a trained Pnet to locate a landmark, and it can be easily reused for locating the bounding box of an organ without additional training. Specifically, with regard to the organ B-box prediction, we transfer it to a landmark localization problem. As shown in Fig. 3, there are two possible methods to implement this. The first is to locate the maximum and minimum coordinates of B-box among three dimensions by predicting bottom-left corner and top-right corner  $[D_{min}, D_{max}]$ , as suggested by [9], which is referred to as "Diagonal Points" as shown in Fig. 3(a). However, these two points may not be associated with the wanted organ, and could even be located in meaningless areas (e.g., air background). As the case shown in Fig. 3(c), the minimum diagonal point  $D_{min}$  of mandible is in the air background, which is hard to detect due to lack of contextual information. Therefore, linking patches directly with the wanted organ would be more reasonable. Alternatively, we propose to locate the six extreme points on the surface of an organ along x, y and z axes, and they are denoted as  $[Z_{min}, Z_{max}, X_{min}, X_{max}, Y_{min}, Y_{max}]$  in Fig. 3(b). This method is referred to as "Extreme Points". As shown in Fig. 3(c), using the the extreme points can ensure these landmarks to be located in the body foreground and avoid locating points in the air background, thus more contextual information can be leveraged to locate the landmarks and obtain more accurate position and scale of the associated B-box.

## 3 Experiments

### 3.1 Dataset and Evaluation Metrics

The proposed method was evaluated on a mixed head and neck (HaN) CT dataset containing 165 volumes from three sources equipped with varying hard-

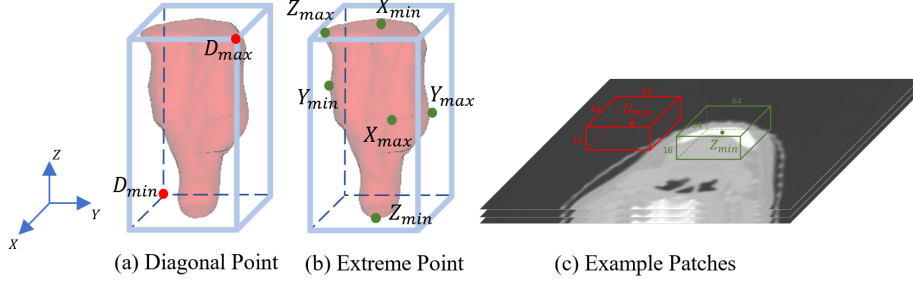


Fig. 3: Example of two methods transferring B-box estimation to points localization: (a) Directly locating the bottom-left corner and top-right corner of B-box; (b) Finding 6 extreme points along x, y, and z axes; (c) An example of the two different types of points and their surrounding patches of mandible. The patch around  $D_{min}$  (minimum diagonal point) locates at meaningless area (air), while the one around  $Z_{min}$  (minimum extreme point along axial orientation) links directly to the bound of the mandible.

ware: 50 patients from StructSeg 2019, 48 patients from MICCAI 2015 Head and Neck challenge [13] and 67 patients collected locally with nasopharyngeal carcinoma before radiotherapy treatment. Since these three datasets were originally annotated with organs masks and had different set of labeled organs, we used four organs that were annotated in all of them: brain stem, mandible, left and right parotid gland. For scans from StructSeg 2019 and locally collected, their inter-slice and intra-slice spacings are all around 1mm and 3mm. And for scans from MICCAI 2015 Head and Neck challenge, their inter-slice spacing was isotropic, and varied between 0.76 mm and 1.27mm. The spacing in each volume was resampled to  $3 \times 1 \times 1$  mm along axial, coronal, sagittal directions and cropped to remove the air background. The 165 volumes were splitted into 109 training, 19 validation and 38 testing samples. As our model does not need any annotation during the *training* stage, we abandoned all the annotations in the training set. The ground truth 3D B-boxes and extreme points in the validation and testing images were inferred from the 3D masks of each organ. While during the *inference* stage, we use a randomly selected image from the validation set as the support (reference) image, and use each image in the testing set as the query image, respectively. For the direct comparison of different methods, we calculated the widely reported metric Intersection over Union (IoU) overlap ratio between the predicted B-box and the ground-truth B-box. the IoU overlap ratio is defined as:

$$IoU = \frac{B_p \cap B_{gt}}{B_p \cup B_{gt}} \quad (4)$$

where  $B_p$  and  $B_{gt}$  denote the predicted B-box and the ground-truth B-box, respectively. And we also calculate the Absolute Wall position (AWD) for comparison following [7, 16].

### 3.2 Implementation Details

Our model was trained and tested on a Ubuntu desktop with an NVIDIA GTX 1080 Ti GPU. The Adam optimizer [8] was used for training with batch size 6, initial learning rate  $10^{-3}$ , weight decay  $10^{-8}$ , and 250 epochs. The learning rate was decayed by 0.9 every 10 epochs. The coarse and fine model  $M_c$ ,  $M_f$  are trained separately as described in Section 2.2. With regard to every query volume, we choose  $K = 15$  and constrain each initial position in the non-air region, in order to avoid sampling outside the meaningful area. A fixed patch size of  $16 \times 64 \times 64$  pixels is used for support and query patches during locating all the extreme points for the organ detection problem. The code is available: <https://github.com/LWHYC/RPR-Loc>.

### 3.3 Experiment Results

**Performance of organ localization and multi-run ensemble** As we transfer an organ detection problem into a set of landmark detection problems, we first compare the two different landmark representation strategies: "Diagonal Points" and "Extreme Points". We also investigate the effect of hyper-parameter  $K$  for multi-run ensemble on the localization performance. As shown in Tab. 1, with one initial patch, predicting extreme points rather than diagonal points can prominently increase IoU value and reduce AWD for all organs, especially for the mandible. Because in different volumes, the diagonal points on the bounding box may be in distinct tissues such as the air background and difficult to locate, thus the performance of B-box prediction is limited in this strategy. Therefore, we apply the "extreme points" location strategy for all subsequent experiments.

Last five rows of Tab. 1 show that the average accuracy will also increase obviously as the number runs for multi-run ensemble increases from 1 to 15 and stops at 20. This is in line with our expectations that taking average of predictions from different start points would increase the precision and robustness of our model.

**Performance of multi-step localization** Based on the "extreme points" strategy for organ detection and with  $K = 15$ , we report the effectiveness of our multi-step model in Tab. 2. Moving the agent by two or three steps with coarse model  $M_c$  achieves better results than just one step. However, using  $M_c$  by three steps almost leads to no improvement compared with using  $M_c$  by two steps. In contrast, using  $M_c$  in the first step followed by using  $M_f$  in the second step achieved the best performance, which improved the average IoU by 6% and reduced the average AWD by 1.3 mm compared with only using  $M_c$  for one step. It shows that fine model  $M_f$  trained within small offset range  $r$  could deal with the movements of small steps more effectively.



Table 1: The mean organ localization IoU (% , left) and AWD (mm, right) of four HaN OARs under different strategies and different numbers of multi-run ensemble (MRE) with our coarse model. "Diagonal" and "Extreme" mean organ detection via localization of diagonal points and extreme points, respectively.

strategy	MRE	Brain stem	Mandible	L Parotid	R Parotid	Mean
Diagonal	1	44.5, 7.06	32.3, 15.29	36.5, 9.94	35.7, 9.66	37.2, 10.49
Extreme	1	45.9, 6.61	62.2, 8.04	38.6, 9.61	37.5, 9.09	46.1, 8.34
Extreme	5	49.4, 5.63	62.7, 7.52	41.8, 8.66	36.8, 9.13	47.7, 7.73
Extreme	10	50.8, 5.34	63.2, 7.40	42.4, 8.73	38.4, 8.88	48.7, 7.59
Extreme	15	50.7, 5.34	<b>63.7, 7.28</b>	<b>43.1, 8.48</b>	<b>38.8, 8.79</b>	<b>49.1, 7.48</b>
Extreme	20	<b>51.9, 5.16</b>	63.3, 7.45	42.6, 8.57	37.4, 9.03	48.8, 7.55

Table 2: The mean localization IoU (% , left) and AWD (mm, right) of four HaN OARs of different multi-step methods.

Method	Brain stem	Mandible	L Parotid	R Parotid	Mean
$M_c$ (one step)	50.7, 5.34	63.7, 7.28	43.1, 8.48	38.8, 8.79	49.1, 7.48
$M_c$ (two steps)	51.4, 5.30	68.0, 6.03	45.0, 8.23	38.7, 8.89	50.7, 7.11
$M_c$ (three steps)	50.5, 5.52	68.7, 5.79	<b>45.3, 8.30</b>	38.9, 8.81	50.9, 7.10
$M_c + M_f$	<b>61.5, 3.70</b>	<b>70.0, 5.39</b>	44.8, <b>7.74</b>	<b>44.2, 7.65</b>	<b>55.1, 6.12</b>

**Comparison with other methods** In this section, we compare our method with template matching-based alternatives for the one-shot organ localization under the same setting as our method. Same as Section 2.3, we transfer B-box localization task to localization of the corresponding extreme points. We crop patches of size  $16 \times 64 \times 64$  pixels around each extreme point from the support volume, then implement template matching method by sliding window operation with stride 2 along each dimension to find the patch in the test image that is the most similar to the support patch. We consider the following similarity-based methods for comparison:

1) Gray Scale MSE (GS MSE). We directly compute the similarity between each of the query patch and the support patch cropped from the original gray scale images, and MSE is adopted as similarity criteria.

2) Gray Scale (GS Cosine), which means using cosine similarity as criteria for comparison and it is defined as:

$$Sim(\mathbf{x}_q, \mathbf{x}_s) = \frac{\mathbf{x}_q \cdot \mathbf{x}_s}{\|\mathbf{x}_q\| \|\mathbf{x}_s\|} \quad (5)$$

where  $\mathbf{x}_q$  is the query patch and  $\mathbf{x}_s$  is the support patch.

3) Gray Scale Normalized Cross Correlation (GS NCC). Cross correlation is a measure of similarity of two series in signal processing, we use normalized cross correlation to evaluate the similarity of support and query patches. It can be defined as:

$$Sim(\mathbf{x}_q, \mathbf{x}_s) = \frac{Cov(\mathbf{x}_q, \mathbf{x}_s)}{\sqrt{Var(\mathbf{x}_q)Var(\mathbf{x}_s)}} \quad (6)$$

where  $\text{Cov}(\cdot, \cdot)$  means the covariance and  $\text{Var}(\cdot)$  means the variance.

4) Feature Map MSE (FM MSE). An auto-encoder network [10] was trained to transform a patch into a latent low-dimensional feature vector, as we use MSE between the corresponding latent features to measure similarity between support and query patches.

5) Feature Map Cosine (FM Cosine). Similarly to GS Cosine method, we use cosine similarity between latent features obtained by the above auto-encoder for similarity measurement.

We successively conduct experiments to compare the performance of our proposed method with that of other similarity-based methods. With the same query volume, Tab. 3 shows comparison of these methods on accuracy and average time consumption for each organ. Our method outperforms GS MSE, GS Cosine, GS NCC and FM MSE by an average IoU score of  $>7\%$  and AWD of  $>2\text{mm}$ . Despite FM Cosine slightly outperformed our method in terms of IoU of the right parotids, its performance is much lower on the brain stem, and the average accuracy across the four organs is also much lower than ours. In addition, the alternative methods are based on sliding window scanning, which is time consuming. Our method only requires 0.15s for localization of one organ, which is  $1.7 \times 10^5$  times faster than FM Cosine.

Table 3: The mean localization IoU (% , left), AWD (mm, right) of four HaN OARs and the average inference time for each OAR of different methods.

Method	Brain stem	Mandible	L Parotid	R Parotid	Mean	Time(s)
Ours	<b>61.5, 3.70</b>	<b>70.0, 5.39</b>	<b>44.8, 7.74</b>	44.2, <b>7.65</b>	<b>55.1, 6.12</b>	<b>0.15</b>
GS MSE	39.3, 7.47	65.7, 7.20	39.8, 10.67	37.1, 10.67	45.5, 9.00	1052.96
GS Cosine	35.2, 7.83	67.4, 7.10	36.9, 11.07	36.7, 10.30	44.1, 9.08	1421.60
GS NCC	46.9, 7.35	58.9, 9.76	24.3, 18.78	23.9, 20.14	38.5, 14.01	4547.80
FM MSE	44.7, 6.52	67.7, 6.88	39.2, 10.43	40.6, 8.79	48.1, 8.16	26586.24
FM Cosine	50.2, 5.91	69.1, 5.53	44.7, 7.97	<b>44.6</b> , 8.22	52.2, 7.92	25976.32

As shown in Fig. 4, despite the large variation in shapes and low contrast to surrounding tissues, the proposed framework could accurately locate B-box in the query volume. This implies that the proposed relative position or offset-based regression method has successfully trained the network to infer the offset from a random patch to a target position.

## 4 Discussion & Conclusions

In this work, we propose a relative position regression-based one-shot localization framework (RPR-Loc) for medical images, which to our best knowledge is the first work of one-shot localization in volumetric medical scans. Note that our one-shot localization can be easily extended to few-shot localization given multiple support volumes. Opposed to the traditional time-consuming template

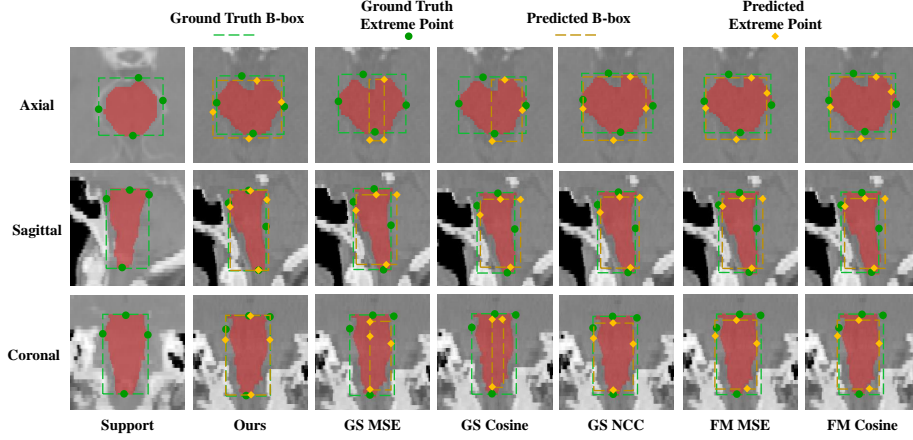


Fig. 4: Qualitative localization results of brain stem in a query volume on three dimensions. The proposed method achieves desirable results which are close to the ground truth.

matching methods, our framework is regression-based thus not sensitive to the volume size and could located the wanted landmark/organ in a short time. Although reinforcement learning-based methods [1, 6] also locate the landmarks by offset prediction, their need a large set of annotated images, could only locate a fixed set of landmarks, and require a very long training time due to learning from episodes. In contrast, our method does not need any annotation during the training stage and could be employed to locate any landmarks or organs contained in the training dataset during the inference stage. By learning to predict relative positions of two patches from the same volume, our method can locate the target position in the query volume by moving the initial agent. Results on multi-organ localization from head and neck CT volumes showed that our method achieved more accurate results and is more than  $10^5$  times faster than template matching methods under the same setting. This study demonstrates the effectiveness of our PRP-Loc in reducing annotations for medical image analysis, and it is of interest to apply it to other organs in the future.

**Acknowledgement** This work was supported by the National Natural Science Foundations of China [81771921, 61901084] funding.

## References

1. Alansary, A., Oktay, O., Li, Y., Le Folgoc, L., Hou, B., Vaillant, G., Kamnitsas, K., Vlontzos, A., Glocker, B., Kainz, B., et al.: Evaluating reinforcement learning agents for anatomical landmark detection. *Medical image analysis* 53, 156–164 (2019)

2. Bart, E., Ullman, S.: Cross-generalization: Learning novel classes from a single example by feature replacement. In: 2005 IEEE Computer Society Conference on Computer Vision and Pattern Recognition (CVPR'05). vol. 1, pp. 672–679. IEEE (2005)
3. Brunelli, R.: Template matching techniques in computer vision: theory and practice. John Wiley & Sons (2009)
4. Fei-Fei, L., Fergus, R., Perona, P.: One-shot learning of object categories. *IEEE transactions on pattern analysis and machine intelligence* 28(4), 594–611 (2006)
5. Forbes, G.B.: Human body composition: growth, aging, nutrition, and activity. Springer Science & Business Media (2012)
6. Ghesu, F.C., Georgescu, B., Zheng, Y., Grbic, S., Maier, A., Hornegger, J., Comaniciu, D.: Multi-scale deep reinforcement learning for real-time 3d-landmark detection in ct scans. *IEEE transactions on pattern analysis and machine intelligence* 41(1), 176–189 (2017)
7. Humpire Mamani, G., Setio, A., Ginneken, B., Jacobs, C.: Efficient organ localization using multi-label convolutional neural networks in thorax-abdomen ct scans. *Physics in Medicine and Biology* 63 (03 2018)
8. Kingma, D.P., Ba, J.: Adam: A method for stochastic optimization. *arXiv preprint arXiv:1412.6980* (2014)
9. Law, H., Deng, J.: Cornernet: Detecting objects as paired keypoints. In: *Proceedings of the European Conference on Computer Vision (ECCV)*. pp. 734–750 (2018)
10. Lei, W., Wang, H., Gu, R., Zhang, S., Zhang, S., Wang, G.: Deepigeos-v2: Deep interactive segmentation of multiple organs from head and neck images with lightweight cnns. In: *Large-Scale Annotation of Biomedical Data and Expert Label Synthesis and Hardware Aware Learning for Medical Imaging and Computer Assisted Intervention*, pp. 61–69. Springer (2019)
11. Li, X., Yu, L., Jin, Y., Fu, C.W., Xing, L., Heng, P.A.: Difficulty-aware meta-learning for rare disease diagnosis. In: *International Conference on Medical Image Computing and Computer-Assisted Intervention*. pp. 357–366. Springer (2020)
12. Oquab, M., Bottou, L., Laptev, I., Sivic, J.: Is object localization for free?-weakly-supervised learning with convolutional neural networks. In: *Proceedings of the IEEE conference on computer vision and pattern recognition*. pp. 685–694 (2015)
13. Raudaschl, P.F., Zaffino, P., Sharp, G.C., Spadea, M.F., Chen, A., Dawant, B.M., Albrecht, T., Gass, T., Langguth, C., Lüthi, M., et al.: Evaluation of segmentation methods on head and neck ct: auto-segmentation challenge 2015. *Medical physics* 44(5), 2020–2036 (2017)
14. Vlontzos, A., Alansary, A., Kamnitsas, K., Rueckert, D., Kainz, B.: Multiple landmark detection using multi-agent reinforcement learning. In: *International Conference on Medical Image Computing and Computer-Assisted Intervention*. pp. 262–270. Springer (2019)
15. Wang, D., Zhang, Y., Zhang, K., Wang, L.: Focalmix: Semi-supervised learning for 3d medical image detection. In: *Proceedings of the IEEE/CVF Conference on Computer Vision and Pattern Recognition*. pp. 3951–3960 (2020)
16. Xu, X., Zhou, F., Liu, B., Fu, D., Bai, X.: Efficient multiple organ localization in ct image using 3d region proposal network. *IEEE transactions on medical imaging* 38(8), 1885–1898 (2019)
17. Zhang, J., Liu, M., Shen, D.: Detecting anatomical landmarks from limited medical imaging data using two-stage task-oriented deep neural networks. *IEEE Transactions on Image Processing* 26(10), 4753–4764 (2017)